Journal of Molecular Structure 1205 (2020) 127655

Contents lists available at ScienceDirect

Journal of Molecular Structure

journal homepage: http://www.elsevier.com/locate/molstruc

Synthesis, DFT calculations and molecular docking study of mixed ligand metal complexes containing 4,4′-dimethyl-2,2′-bipyridyl as α-glucosidase inhibitors

Davut Avcı [a, *], Sümeyye Altürk [a], Fatih Sönmez [b], Ömer Tamer [a], Adil Başoğlu [a], Yusuf Atalay [a], Belma Zengin Kurt [c]

[a] Sakarya University, Faculty of Arts and Sciences, Department of Physics, 54187, Sakarya, Turkey
[b] Sakarya University of Applied Sciences, Pamukova Vocational School, 54055, Sakarya, Turkey
[c] Bezmialem Vakif University, Faculty of Pharmacy, Department of Pharmaceutical Chemistry, 34093, Istanbul, Turkey

ARTICLE INFO

Article history:
Received 25 October 2019
Received in revised form
2 December 2019
Accepted 26 December 2019
Available online 31 December 2019

Keywords:
4,4′-dimethyl-2,2′-bipyridyl and
6−methylpyridine−2−carboxylic acid
LC-MS/MS
FT−IR and UV−Vis
α-Glucosidase
HSEh1PBE

ABSTRACT

Novel mixed ligand metal complexes including 4,4′-dimethyl-2,2′-bipyridyl (dmdpy) and 6-methylpyridine-2-carboxylic acid (6-mpaH) {[VO(6-mpa)(dmdpy)]·SO_3, (**1**), [Fe(6-mpa)(dmdpy)$(NO_3)_2$]·NO_3, (**2**), Ni(6-mpa)(dmdpy)Cl_2, (**3**), [Zn(6-mpa)(dmdpy)Cl_2]·H_2O, (**4**), Cd(6-mpa)$_2$(dmdpy), (**5**), [Hg(6-mpa)(dmdpy)$(NO_3)_2$]·H_2O, (**6**)} were synthesized as potential α-glucosidase inhibitors. Their structural characterizations, vibrational and electronic spectral behaviours were investigated by elemental analysis, LC-MS/MS, FT−IR and UV−Vis spectroscopic techniques. The inhibitory activities of these complexes against α-glucosidase (from *Saccharomyces cerevisiae*, EC No: 3.2.1.20) were determined. The synthesized complexes **1**−**6** exhibited α-glucosidase inhibitory activity with the IC_{50} values ranging from 0.4699 to >600 μM. Besides, density functional theory (DFT) calculations in the mode of hybrid HSEh1PBE method with 6-311G(d,p) and LanL2DZ basis sets for optimal complex geometries were fulfilled to obtain the vibrational frequencies and electronic spectral behaviours as well as substantial contributions to the electronic transitions. Furthermore, the molecular docking study was performed to examine protein-ligand interactions between the synthesized complexes (**1**−**6**) and target protein (the template structure *S. cerevisiae* isomaltase (PDBID: 3A4A)).

Author contribution statement

Davut Avcı: Investigation; Methodology; Project administration; Writing-Original draft preparation; Writing-review & editing; Supervision.
Sümeyye Altürk: Data curation.
Fatih Sönmez: Investigation; Methodology; Review & editing.
Ömer Tamer: Formal analysis; Review & editing.
Adil Başoğlu: Methodology.
Yusuf Atalay: Software.
Belma Zengin Kurt: Methodology.

1. Introduction

Metal complexes of the ligands including heteroatom have been frequently used for the field of coordination chemistry because their structural, spectroscopic and catalytic properties are similar to some enzyme-substrate complexes in our bodies [1–5]. Due to many applications in material and medicinal chemistry, synthesis of pyridine derivatives (pyridine-2-carboxylic acid, 3-/6-methylpyridine-2-carboxylic acid, 2,2′-bipyridyl, 4,4′-dimethyl-2,2′-bipyridyl, etc.) and their different coordination complexes are important for the investigations of physicochemical properties such as catalysis, nonlinear optics, luminescence, etc., and biological and pharmaceutical activities [6–15]. The investigations of the effective treatments for diabetes mellitus type 2 (T2DM) are still important in the literature. Since glucose control is an effective treatment for diabetes, digestive enzymes such as α−glucosidase or α−amylase in the intestinal should be inhibited to slow down sugar digestion and absorption. The influential antidiabetic remedies

* Corresponding author.
E-mail address: davci@sakarya.edu.tr (D. Avcı).

https://doi.org/10.1016/j.molstruc.2019.127655
0022-2860/

purpose for decreasing blood glucose levels and keeping glucose under control. According to recent studies [4,16], it could be said that α-glucosidase inhibitor (AGI) improves postprandial hyperglycemia and subsequently reduces the risk of developing type 2 diabetes in patients. α-Glucosidase (EC 3.2.1.20) is a critical enzyme for the digestion of carbohydrates, it catalyzes the cleavage of absorbable monosaccharides, beginning from disaccharides and oligosaccharides [17]. It is well known that the inhibitions of α-glucosidase and related enzymes take part in a role in the treatment of diabetes, cancer, human immunodeficiency virus (HIV/AIDS) and other degenerative diseases, etc. [18,19]. To treat T2DM, some of AGIs (acarbose, voglibose, and miglitol, etc.) are clinically used [20]. There are a few AGIs commercially available in pharmacies, but they are inadequate as necessary effective treatments due to side effects. Hence, the synthesis and design of high-affinity glucosidase inhibitors have been collected great attention in the whole world. In order to fulfill this goal, many natural and synthetic heterocyclic compounds (benzothiazole, xanthones, flavonoid, pyrrolidine, indole analogues, etc.) have been explored over the years as α-glucosidase inhibitors [4,16,21–23].

As a consequence of our ongoing works, the aim of this paper is the synthesis of effective complexes including different metal ions playing the role on the healing effect on people with type 2 diabetes as potential α-glucosidase inhibitors. Novel metal complexes (complexes **1**–**6**) containing 6-methylpyridine-2-carboxylic acid (6-mpaH) and 4,4′-dimethyl-2,2′-bipyridyl (dmbpy) were synthesized. The complex structures of V(IV), Fe(II), Ni(II), Zn(II), Cd(II) and Hg(II) were determined by mass spectrometry (MS), FT-IR spectra and elemental analysis. The investigation of α-glucosidase enzyme inhibition and spectral behaviours were experimentally performed. In addition, the structural, spectral and electronic properties, as well as first- and second-order hyperpolarizability parameters of complexes **1**–**6** in the gas phase and ethanol were examined by using DFT/HSEh1PBE/6-311G(d,p)/LanL2DZ level. The detailed investigation of the interactions between the synthesized complexes and protein was also evaluated with molecular docking.

2. Experimental and computational details

2.1. Materials and physical measurements

All of the chemical reagents used in this study are analytical grade commercial products. 6-mpaH (6-methylpyridine-2-carboxylic acid), and 4,4′-dimethyl-2,2′-bipyridyl (dmbpy), vanadium(IV) oxide sulfate hydrate ($VOSO_4 \cdot xH_2O$), iron(III) nitrate nonahydrate ($Fe(NO_3)_3 \cdot 9H_2O$), nickel(II) chloride ($NiCl_2$), zinc(II) chloride ($ZnCl_2$), cadmium(II) acetate ($Cd(OAc)_2$) and mercury(II) nitrate monohydrate ($Hg(NO_3)_2 \cdot H_2O$) were purchased from Sigma-Aldrich.

The details of the spectrophotometers used to record LC-MS/MS, FT-IR, UV–Vis spectra are given in the Supplementary Material.

2.2. Synthesis of the complexes 1–6 {[VO(6-mpa)(dmdpy)]·SO_3, (1), [Fe(6-mpa)(dmdpy)$(NO_3)_2$]·NO_3, (2), Ni(6-mpa)(dmdpy)Cl_2, (3), [Zn(6-mpa)(dmdpy)Cl_2]·H_2O, (4), Cd(6-mpa)$_2$(dmdpy), (5), [Hg(6-mpa)(dmdpy)$(NO_3)_2$]·H_2O, (6)}

The synthesis methods of the complexes 1–6 are as follows (see Scheme 1):

Synthesis of the complex **1:** The 4,4′-dimethyl-2,2′-bipyridyl (1 mmol) and vanadium(IV) oxide sulfate hydrate (1 mmol) were added to a mixture of ethanol and water (15 ml, 1:1), the mixture was stirred within closed vial at 60 °C for 2 h. Then 6-methylpyridine-2-carboxylic acid (1 mmol) was added to this mixture and stirred for 2 h, and evaporated for 18 days at room temperature. The powder product for complex **1** was filtered off, washed thoroughly with distilled water, and finally air-dried at room temperature. Anal. Calc. for $C_{19}H_{18}N_3O_6SV$ (complex **1**): C, 48.83; H, 3.88; N, 8.99. Exact mass (*m*/*z*): 467.0356. Found: C, 48.82; H, 3.85; N, 8.99; S, 6.85. ESI-LC-MS/MS (*m*/*z*): 467.1 ($[M]^+$). The mass spectrum for complex **1** is given in Fig. S1.

Synthesis of the complexes **2,6:** The iron(III) nitrate nonahydrate (1 mmol for complex **2**)/mercury(II) nitrate monohydrate (1 mmol for complex **6**), 4,4′-dimethyl-2,2′-bipyridyl (1 mmol) and 6-methylpyridine-2-carboxylic acid (1 mmol) were added to a mixture of acetonitrile and water (20 ml, 1:1), respectively. The solution was stirred within closed vial at 70 °C for 5 h, and evaporated for 10 days at room temperature. At the end of this process, the powder products for complex **2** and **6** were filtered off, washed thoroughly with distilled water, and finally air-dried at room temperature. Anal. Calc. for $C_{19}H_{18}N_6O_{11}Fe$ (complex **2**): C, 40.59; H, 3.23; N, 14.95. Exact mass (*m*/*z*): 562.0383. Found: C, 40.57; H, 3.20; N, 14.95; ESI-LC-MS/MS (*m*/*z*): 562.3 ($[M]^+$). Anal. Calc. for $C_{19}H_{20}N_5O_9Hg$ (complex **6**): C, 34.42; H, 3.04; N, 10.56. Exact mass (*m*/*z*): 664.0967. Found: C, 34.33; H, 3.01; N, 10.54; ESI-LC-MS/MS (*m*/*z*): 665.5 ($[M]^+$). The mass spectra for complexes **2** and **6** are given in Figs. S2 and S3, respectively.

Synthesis of the complexes **3,4:** The 6-methylpyridine-2-carboxylic acid (1 mmol), nickel(II) chloride (1 mmol for complex **3**)/zinc(II) chloride (1 mmol for complex **4**) and 4,4′-dimethyl-2,2′-bipyridyl (2 mmol) were added to a mixture of ethanol and water (20 ml, 1:1) at 70 °C. After the mixture was refluxed for 24 h (complex **3**) and 3 h (complex **4**), respectively, they were allowed to evaporate at room temperature. After the period of a week, the powder products for complexes **3,4** were filtered off, washed thoroughly with distilled water, and finally air-dried at room temperature. Anal. Calc. for $C_{19}H_{20}Cl_2N_3O_3Ni$ (complex **3**): C, 48.76; H, 4.31; N, 8.98. Exact mass (*m*/*z*): 466.0235. Found: C, 48.88; H, 4.29; N, 9.01; ESI-LC-MS/MS (*m*/*z*): 471.1 ($[M+4H]^+$). Anal. Calc. for $C_{19}H_{20}Cl_2N_3O_3Zn$ (complex **4**): C, 48.08; H, 4.25; N, 8.85. Exact mass (*m*/*z*): 472.0173. Found: C, 48.30; H, 4.23; N, 8.89; ESI-LC-MS/MS (*m*/*z*): 477.1 ($[M+4H]^+$). The mass spectra for complexes **3** and **4** are given in Figs. S4 and S5, respectively.

Synthesis of the complex **5:** The cadmium(II) acetate (1 mmol), 4,4′-dimethyl-2,2′-bipyridyl (1 mmol) and 6-methylpyridine-2-carboxylic acid (2 mmol) were added to a mixture of ethanol and water (30 ml, 1:1) at 50 °C. The mixture was stirred at 50 °C for 2 h and evaporated for three weeks at room temperature. At the end of this process, the powder product for complex **5** was filtered off, washed thoroughly with distilled water, and finally air-dried at room temperature. Anal. Calc. for $C_{26}H_{24}N_4O_4Cd$ (complex **5**): C, 54.89; H, 4.25; N, 9.85. Exact mass (*m*/*z*): 570.0831. Found: ESI-LC-MS/MS (*m*/*z*): 596.5 ($[M+Na]^+$). The mass spectrum for complex **5** is given in Fig. S6.

2.3. α-Glucosidase inhibition assay

According to our previous studies [19,24,25], α–glucosidase inhibition activities of the synthesized complexes (**1**–**6**) were determined. The detailed inhibition method is presented in Supplementary Material. The investigation of α–glucosidase (from *Saccharomyces cerevisiae*, EC No: 3.2.1.20) inhibition activities for the complexes **1**–**6** was performed by following equation;

$$\text{Glucosidase inhibition} = [(A_c - A_s)/A_c]x100$$

where A_c is the absorbance of control and A_s is the absorbance of samples, respectively. The calculation of IC_{50} values was fulfilled by using Graphpad Software.

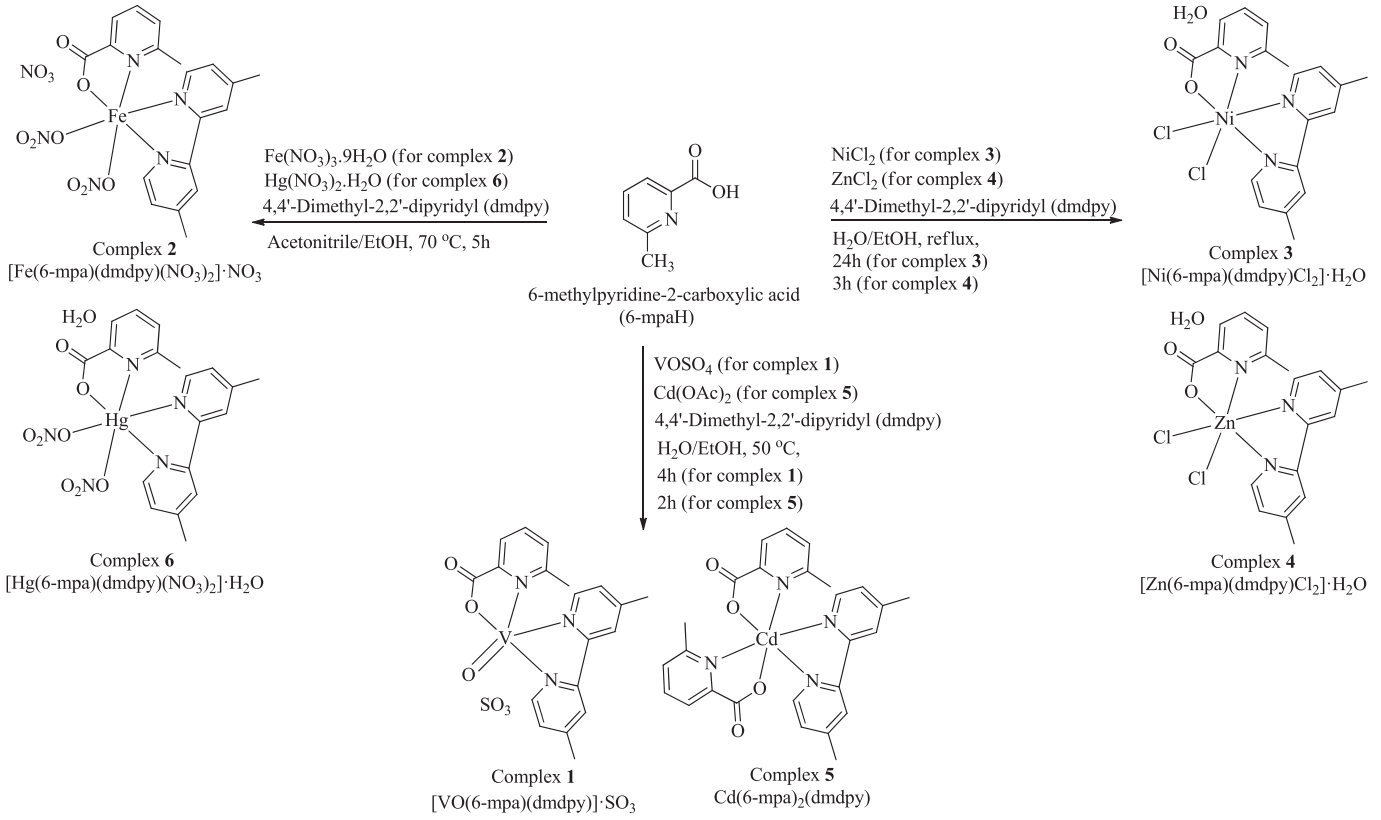

Scheme 1. The synthesis of the complexes **1**–**6**.

2.4. Computational procedure

All quantum chemical calculations of the synthesized complexes (**1**–**6**) were performed by using GAUSSIAN 09, Revision D01 [26], and GaussView 5 program [27].

The spin-restricted DFT calculations were fulfilled for the complexes **1,2,5** containing V, Fe, Cd ions, while the unrestricted DFT calculations were carried out for the complexes **3,4,6** containing Ni, Zn, Hg ions, respectively. The stable spin states for the complexes **1,2,5** including V, Fe, Cd ions are singlet and for the complexes **3,4,6** including Ni, Zn, Hg are doublet.

The complex geometries with various spin configurations were optimized and the lowest energy structures for the complexes **1**–**6** were chosen for further analysis.

The optimized complex structures and vibrational frequencies of the complexes **1**–**4** were obtained at the DFT/HSEh1PBE hybrid density functional [28,29] and the combined basis set of 6-311G(d,p) [30] for C, N, O, H atoms, and LanL2DZ [31] for V, Fe, Ni and Zn atoms. The same parameters for complexes **5** and **6** were investigated by using DFT/HSEh1PBE/LanL2DZ level. The time−dependent DFT (TD−DFT) level [32] with the conductor−like polarizable continuum model (CPCM) [33] was applied to examine the electronic spectral behaviours of complexes **1**–**6** in the ethanol and gas phase. The other molecular parameters were computed by using the same level.

2.5. Docking procedure

The molecular docking was fulfilled by using the iGEMDOCK program [34], so as to survey protein-ligand interactions between the synthesized complexes (**1**–**6**) and target protein (the template structure *S. cerevisiae* isomaltase) used as rigid. Before the ligand-protein interaction calculations, the beginning ligand structures were selected by basis on the ground state structures of the complexes **1**–**6** obtained by GAUSSIAN program. GEMDOCK parameters in the flexible docking were applied by considering the sequential conditions: The initial step sizes ($\sigma = 0.8$ and $\psi = 0.2$; step-size vectors of decreasing-based Gaussian mutation and self-adaptive Cauchy mutation, respectively), family competition length ($L = 2$), population size ($N = 800$), and recombination probability ($p_c = 0.3$). GEMDOCK optimization was chosen to complete when convergence falls below a certain threshold or reaches a maximum of 80 pre-set values for each ligand screened. Hence, GEMDOCK supplies 800 solutions in a generation and then terminates the calculation after completing 64000 solutions for each inserted ligand.

3. Results and discussion

3.1. Analysis of molecular geometries of the synthesized complexes (*1*–*6*)

The chemical geometric structures of the synthesized complexes (**1**–**6**) were estimated by FT-IR spectra and DFT calculations. Moreover, their molecular formulas were confirmed by mass spectrometry (MS) and elemental analysis. Fig. S7 depicts the optimized theoretical molecular structures of the complexes **1**–**6**. The coordination geometry around V(IV) metal for complex **1** is described as a distorted square-bipyramidal, whereas the coordination around M(II) atom for the complexes **2**–**6** are determined as distorted octahedral geometry. In the complexes **2**–**5**, while the environment of the central Ni(II) and Zn(II) ions for the complexes **3** and **4** are coordinated by 6-mpa, dmbpy and two chlorine atoms, the environment of the central Fe(II) and Hg(II) ions for the complexes **2** and **6** are coordinated by 6-mpa, dmbpy and two nitrate

ligands. As for complex **5**, the coordination with two 6-mpa and one dmbpy ligand around the central Cd(II) ion was revealed. Unlike these complexes, the complex **1** consists of the central V(IV) ion coordinated by the 6-mpa and dmbpy ligands, and an oxygen atom. For complex **1**, the apical V–O3 bond length is much smaller compared to the equatorial bond lengths due to the Jahn-Teller effect. For complex **2**, considering to the Jahn-Teller effect, the axial bond lengths (Fe-N_{dmbpy} and Fe–$O_{6\text{-}mpa}$) are smaller than the other equatorial Fe-N_{dmbpy} and Fe–$O_{6\text{-}mpa}$ bond lengths. For complexes **3** and **4**, the axial bond lengths (Ni/Zn–N and Ni/Zn–Cl) are smaller than the other equatorial bond lengths owing to the Jahn-Teller effect. For complex **5**, the axial bond length (Cd–$N_{6\text{-}mpa}$) is smaller than the other equatorial Cd-N_{dmbpy} bond length because of the Jahn-Teller effect. According to the Jahn-Teller effect, it is concluded that the axial bond lengths (Hg–$N_{6\text{-}mpa}$ and Hg-$O_{nitrate}$) are larger than the other equatorial Hg-N_{dmbpy} and Hg–$O_{6\text{-}mpa}$ bond lengths in the complex **6**. All complex geometry environments are confirmed by the calculations of structural parameter (bond lengths and angles) for the complexes **1**–**6** (see Table S1). The bond lengths and angles around the coordination environment of metal ions for complexes **1**–**6** are in agreement with the results obtained before [19,24,25,35–39].

Furthermore, the HSEh1PBE/6-311G(d,p)/LanL2DZ level were applied to the natural bond orbital (NBO) calculations for the complexes **1**–**6**. Because NBO analysis allows investigating the interactions between bonds, the coordination environment of metal ions was also confirmed with the conjugative interaction in the molecular system by using NBO analysis. For the understanding of these interactions, the hyperconjugative interaction energies were examined by using the second-order perturbation approach [37–39]. The coordination environment for the complexes **1**–**6** verifies the delocalization effect observed between lone-pair (n) orbitals of oxygen/nitrogen atom and anti-lone-pair (n*) orbitals of metal ions. The delocalization effect shows the coordination environments of the V(IV), Fe(II), Ni(II), Zn(II), Cd(II) and Hg(II) ions for the complexes **1**–**6** appointed as $n \rightarrow n^*$ interactions. These interactions of the complexes **1**–**6** were determined by the calculation of $E^{(2)}$ values described as the stabilization energy. The calculated $E^{(2)}$ values for the complexes **1**–**6** were found at range from 307.96 to 2.70 kcal/mol (see Table S2). The naked Ni^{2+} and Zn^{2+} ions have the natural electron configurations of $3d^8$ and $3d^{10}$. According to NBO analysis, their natural electron configuration changes to [core]$4s^{0.34}3d^{8.21}4p^{0.03}4d^{0.01}$ and [core]$4s^{0.36}3d^{9.97}4p^{0.01}$ in the complexes **3** and **4**, respectively. It was found that the electron configurations of Ni^{2+} and Zn^{2+} in the complexes **3** and **4** are very close to $3d^8$ and $3d^{10}$. The naked Cd^{2+} and Hg^{2+} ions have the natural electron configurations of $4d^{10}$ and $5d^{10}$. Considering NBO results, the natural electron configurations for the Cd^{2+} and Hg^{2+} ions change to [core]$5s^{0.27}4d^{9.99}5p^{0.25}$ and [core]$6s^{0.36}5d^{9.97}6p^{0.24}$ in the complexes **5** and **6**, respectively.

NBO results display that the O–H···O type intermolecular hydrogen bonding interactions for the complexes **3**,**4**,**6** revealed between the carboxylate group of 6-mpa ligand and OH group of water molecules, as can be seen in Table S2. The $E^{(2)}$ values of the complexes **3**,**4**,**6** for these interactions were obtained at 2.70, 3.20 and 5.27 kcal/mol, respectively. In addition, Table S2 demonstrates the remarkable stabilization interactions in the ligands.

3.2. Vibrational frequency

In the analysis of organic, organometallic and inorganic structures, infrared spectroscopy is one of the commonly used spectroscopic methods. The main purpose of this spectroscopy method is to identify and analyse chemical functional groups and the coordination environment around the metal ions for complexes **1**–**6**. To assign the detailed vibrational modes for complexes **1**–**6**, the FT–IR spectra were recorded, and theoretical vibrational frequencies scaled by 0.96 [40] were obtained by HSEh1PBE/6-311G(d,p)/LanL2DZ level. Fig. 1 and Table 1 display the FT–IR spectra of the complexes **1**–**6** and the comparison of experimental and theoretical vibrational frequencies. FT–IR spectra of the complexes **1**–**6** exhibit the bands of carboxylate group instead of the bands of carboxylic acid groups. These bands were assigned as asymmetric/symmetric COO^- stretching modes observed range from 1685/1376 to 1486/1151 cm^{-1} (see Fig. 1b). These modes have a significant role in the coordination environment of metal ions contributing to the formation of a five-member chelate ring. The corresponding theoretical bands were found to be 1765/1361 and 1491/1102 cm^{-1} range. The difference between these modes indicates the coordination for metal ions as a monodentate ligand on the oxygen atom of carboxylate group belonging to 6-mpa ligand. This coordination is confirmed by previous results [19,24,25,41–43]. The experimental/theoretical NO stretching modes belonging to nitrate ligand for complexes **2** and **6** were obtained at 1342/1332 and 1250/1234 cm^{-1}, respectively (see Table 1), this stretching mode is consistent with previously reported results [44,45]. The other stretching and bending vibrational modes belonging 6-mpa, dmbpy, nitrate and water ligands were given in Table 1 with detailed assignments.

3.3. The UV–Vis absorption spectra, frontier molecular orbitals, and molecular surfaces

The UV–Vis spectra of the complexes **1**–**6** in the ethanol were recorded (see Fig. 2). The calculations of the TD–HSEh1PBE/6–311G(d,p)/LanL2DZ level were fulfilled to evaluate in detail for the electronic absorption spectra, substantial electronic transitions and oscillator strengths. Frontier molecular orbitals (FMO) play an important role in defining the molecular reactivity, electrical and optical properties of molecular system. FMOs are known as HOMO (highest occupied molecular orbital) and LUMO (lowest unoccupied molecular orbital). The visualization of molecular orbitals by using quantum mechanical calculations is important to chemical reactions of molecules and UV–Vis spectra, optical and electronic properties. SWizard [46] program was used to calculate notable contributions from FMOs to the electronic transitions. Table 2 indicates comparatively the experimental and theoretical electronic spectral parameters. Metal to metal charge transfer (MMCT), metal to ligand or ligand to metal charge (MLCT) transfer transitions were calculated as theoretical absorption peak displaying the highest electronic absorption wavelength in ethanol. The corresponding peaks for complexes **1**–**4**,**6** in ethanol were obtained at 577 nm with the contribution $H \rightarrow L+1$ (73%), 598 nm with the contribution $H \rightarrow L$ (93%), 587 nm with the contribution $H-2 \rightarrow L\alpha$(77%), 520 nm with the contributions $H-9 \rightarrow L\beta$(27%)/$H-8 \rightarrow L\beta$(14%) and 578 nm with the contributions $H-16 \rightarrow L\beta$(41%)/$H-22 \rightarrow L\beta$(30%), respectively, as can be seen in Table 2. The experimental peak for complex **5** in the ethanol was emerged at 529 nm (see Table 2 and Fig. 2). The $n \rightarrow \pi^*$ and $\pi \rightarrow \pi^*$ transitions demonstrate that metal–ligand and ligand–ligand charge transfers emerged range from 275 to 211, from 349 to 210, from 285 to 227, from 292 to 219, from 275 to 202 and from 299 to 218 nm in ethanol. The corresponding theoretical peaks in the ethanol and gas phase were obtained at similar intervals. The detailed contributions from FMOs were presented in Table 2. Fig. 3 shows that intraligand charge transfers (ILCT) occur at low absorption values of complexes **1**–**6**.

The direct optical band gap energies are calculated by basis on the Tauc and Menth's equation [37,47]. Fig. 4 demonstrates the E_g band gap energy values of the complexes **1**–**6** found to be 5.17, 5.46, 4.92, 5.30, 5.21 and 5.25 eV, respectively. The large energy gap

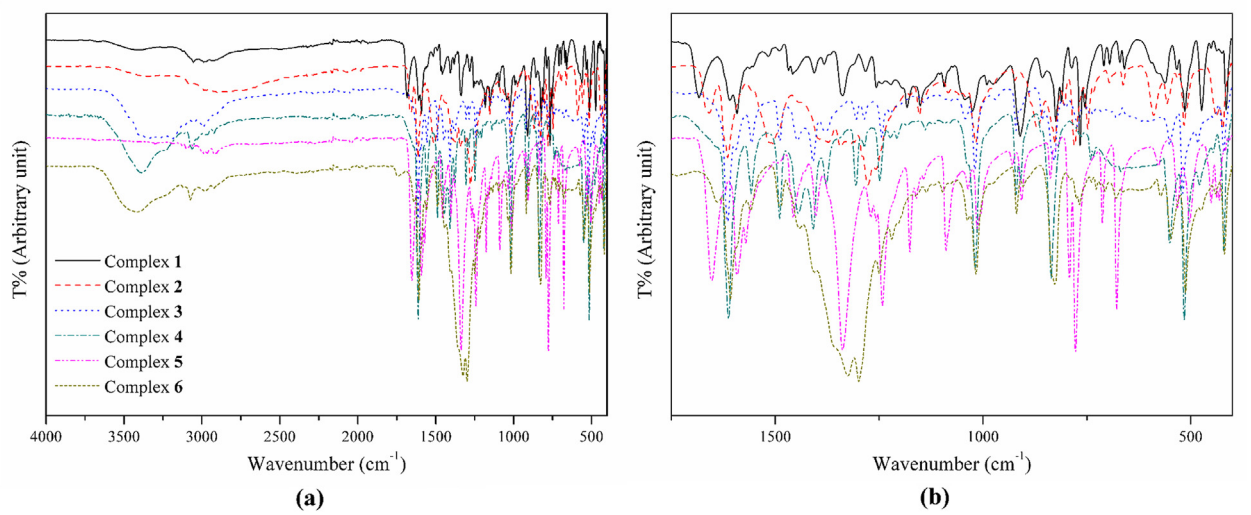

Fig. 1. The FT−IR spectra of the complexes **1**–**6** at the range of (a) 4000−400 cm^{-1}, (b) 1750−400 cm^{-1}.

Table 1
Comparison of the FT−IR and calculated vibration frequencies for the complexes **1**–**6**.

Assignments	Complex **1**		Complex **2**		Complex **3**		Complex **4**		Complex **5**		Complex **6**	
	FT−IR	HSEh1PBE	FT−IR	HSEh1PBE	FT−IR	HSEh1PBE	FT−IR	HSEh1PBE	FT−IR	HSEh1PBE	FT−IR	HSEh1PBE
υ OH	–	–	–	–	3406	3764	3386	3762	–	–	3418	3691
υ OH	–	–	–	–	3338	3543	3234	3498	–	–	3243	3291
υ CH dmdpy	3057	3128	3085	3136	3189	3103	3117	3096	3105	3135	3119	3151
υ CH 6-mpa	2989	3109		3108	3109	3089	3065	3089	3053	3133	3075	3138
υ CH_3 6-mpa	2973	3034	2989	3036	3049	3028	3029	3028	2989	3056	2987	3064
υ CH_3 dmdpy	2937	3022		3027	2993	3026	2973	3024	2964	3056	2971	3060
υ COO^-	1685	1765	1659	1757	1614	1689	1613	1700	1653	1606	1486	1491
υ NO	–	–		1652	–	–	–	–	–	–		
υ CC dmdpy	1609	1612	1613	1626	1557	1625		1622	1593	1608	1607	1613
β HOH	–	–	–	–		1614		1620	–	–		1603
υ CC 6-mpa	1590	1598	1559	1609		1601	1557	1605	1570	1587	1557	1597
β HCC dmdpy	1468	1464		1476	1489	1473	1489	1479		1464	1488	1479
β HCC 6-mpa	1458	1451	1444	1455	1448	1452	1444	1453		1443	1442	1445
β HCH dmdpy		1428		1430		1439		1435	1456	1460		1463
β HCH 6-mpa	1406	1420	1372	1425	1409	1436	1410	1434		1456		1474
υ SO	1338	1321	–	–	–	–	–	–	–	–	–	–
υ NO	–	–	1342	1332	–	–	–	–	–	–	1250	1234
υ NC dmdpy	1282	1313	1278	1300	1287	1299	1286	1302	1258	1308	1298	1314
υ NC 6-mpa	1256	1279	1258	1272	1242	1270	1248	1272	1242	1288	1249	1298
υ COO^-	1151	1102	1318	1319	1307	1333	1376	1361	1270	1314	1324	1328
β ONO	–	–	980	989	–	–	–	–	–	–	1135	1133
υ VO	1043	1070	–	–	–	–	–	–	–	–	–	–
γ HCCC dmdpy	912	946	1017	984	933	980	1017	990	1037	1033	1037	1062
γ HCCC 6-mpa	977	972	923	972	922	942	920	945	1013	1016	1017	1017
β OHO	–	–	–	–	650	658	667	707	–	–	–	–
υ VN	561	548	–	–	–	–	–	–	–	–	–	–
υ NiN	–	–	–	–	550	544	–	–	–	–	–	–
β OSO	514	512	–	–	–	–	–	–	–	–	–	–
γ OOOS	473	492	–	–	–	–	–	–	–	–	–	–
γ CZnCN	–	–	–	–	–	–	447	445	–	–	–	–
γ CNiCN	–	–	–	–	456	444	–	–	–	–	–	–
γ CVCN	437	435	–	–	–	–	–	–	–	–	–	–
υ NiCl	–	–	–	–		399	–	–	–	–	–	–

υ: Stretching; β: in plane bending; γ: out-of plane bending.

between HOMO and LUMO represents a stable structure, while a smaller one represents a more reactive molecule. It is clear from Fig. 3 that the theoretical energy gap calculated from FMO energies were found to be 1.57, 2.32, 3.43 for β spin, 4.31 for α spin, 4.18 and 4.30 for α spin for the complexes **1**–**6**, respectively. Furthermore, the electronegativity (χ), chemical hardness (η) and softness (S) parameters calculated from FMO energies were obtained by previously given equations [37,48]. These parameters of the complexes **1**–**6** were found range from 6.80 for β spin to 3.59 eV, from 2.16 for α spin to 0.14 eV for β spin and from 7.14 for β spin to 0.47 eV^{-1} for α spin, respectively. When the results are evaluated, it could be concluded that complex **1** is more reactive and polarizable than the other complexes **2**–**6**.

Molecular electrostatic potential (MEP) surface, is a useful tool in the investigation of structure-activity and physicochemical properties including chemical, biological and drug molecules, etc. [49,50]. In addition, MEP provides important information about the determination of electron-donating and electron-accepting regions

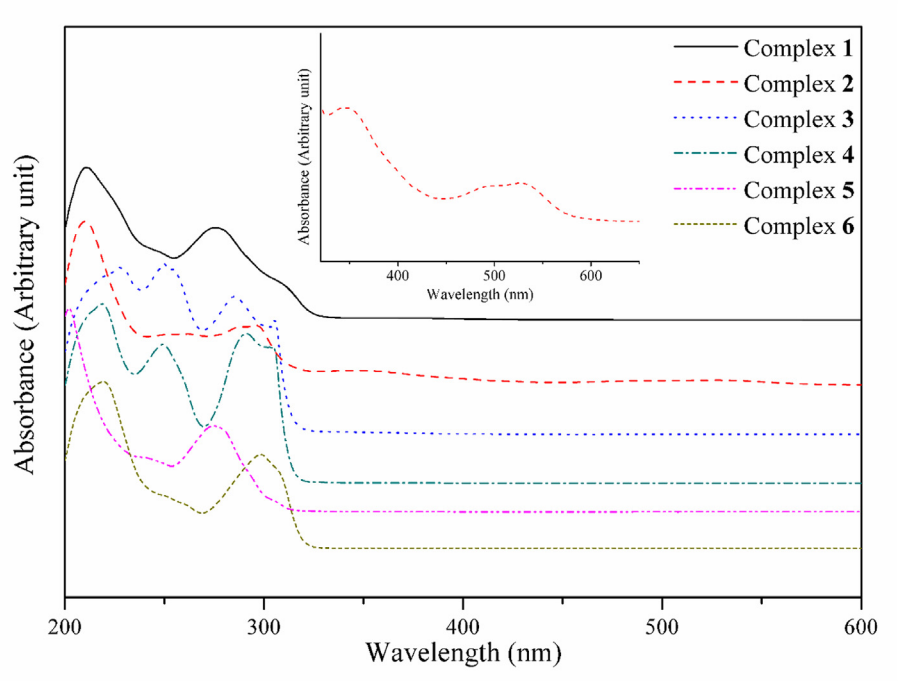

Fig. 2. The UV–vis spectra in ethanol solvent of the complexes **1**–**6.**

in the molecule and about the formation of intra-molecular hydrogen bonds. MEP simultaneously shows the molecular size, shape and electrostatic potential regions in terms of color classification. On the MEP surface, the red color is electron rich, the yellow color is partly electron rich, the blue color is electron deficiency, the light blue color is partially electron deficiency and the green color represents neutral regions. The high red and blue colors on an MEP surface indicate that the molecule under investigation is polar, and colorless or yellow and light blue colors indicate that the polarity of the molecule decreases. Fig. 5 displays the MEP surfaces for complexes **1**–**6** with color code values between the deepest red and blue obtained range from −0.247 to 0.247 a.u., −0.104 to 0.104 a.u., −0.101 to 0.101 a.u., −9.106e−2 to 9.106e−2 a.u., −9.868e−2 to 9.868e−2 a.u. and −7.949e−2 to 7.949e−2 a.u., respectively. The negative regions, which are electrophilic reactivity, are over the electronegative O atoms of the carboxylate groups/uncoordinated water ligands, and the environment of chlorine atoms. The positive regions, which are nucleophilic reactivity, are over the C–H bond surrounding by blue color (see Fig. 5).

3.4. The polarizability, first-order and second-order hyperpolarizability parameters

Due to novel potential applications, such as telecommunication, optical switching and dynamic image processing, etc., the investigation of nonlinear optical (NLO) materials have been taken part in remarkable studies for the last thirty years [51–55]. The discovery of novel materials efficient at technological applications containing organometallic and organic NLO materials is still an important issue at present. Theoretical calculations provide an important contribution to come out the electronic polarization and structure–property relationships of the compound. Lately, it has been reported that the great interest in studying and designing the materials possessing large NLO response, particularly first- and second-order hyperpolarizability [19,24,25,35–37]. In the present study, the HSEh1PBE level was applied to survey the linear optical (LO) and NLO parameters of the complexes **1**–**6** in the gas phase and ethanol, as can be seen in Table 3. By depending on metal ions and their coordination environments, the substantial difference and similarity for all LO and NLO parameters of the complexes **1**–**6** appeared. It could be considered that the presence of Hg metal and nitrate ligands in coordination increased the NLO activity of the complex **6**. Besides, Hg complex is bulkier than the other complexes due to the fact that the atomic diameter of Hg metal is larger than that of Fe, Ni, Zn and Cd metals. The LO (α, $\Delta\alpha$) and NLO (β and γ) parameters of the complexes **1**–**6** in the gas phase and ethanol were obtained from previous equations given references [37,53,54]. The α values of the complexes **1**–**6** in mentioned solvents were found to be range from 85.0×10^{-24} to 42.6×10^{-24} esu. The calculated α values for these complexes were obtained as higher than that of pNA (17×10^{-24} esu). The β values of the complexes **1**–**6** were calculated at the range of 435.1×10^{-30} and 1.0×10^{-30} esu (in the gas phase), 657.7×10^{-30} and 1.9×10^{-30} esu (in the ethanol), respectively. It is noted from Table 3 that the largest β value obtained for the complex **6** in mentioned solvents are of 435.1×10^{-30} and 657.7×10^{-30} esu. To date, in comparison of the complex **6**, we have not obtained the larger β value of metal complexes containing 6-mpa with ciyanate/4(5)Methylimidazole/2,2′-bipyridyl/2,2′-dipyridylamine ligands [19,24,35,36]. This β value displays 3346.92/47.29 and 5059.23/71.49 times higher than those of urea (0.130×10^{-30} esu)/pNA (9.2×10^{-30} esu) [56–58]. Likewise, the γ value of complex **6** in the gas phase calculated at 36214.2×10^{-36} esu is 2414.28 times higher than that of pNA (15×10^{-36} esu) [57,58]. According to the calculated β and γ parameters, it clear that complex **6** exhibits a strong microscopic second–order and third–order NLO property. On the other hand, it could be said that the variation of metals and ligand in coordination affect the results of NLO. In summary, compared to our previous studies on mixed-ligand metal complexes including 6-mpa [19,24,35,36], the complex **6** exhibits the strongest microscopic second–order and third–order NLO activity.

Table 2
Experimental and theoretical electronic transitions, oscillator strength for complexes **1**–**6**.

Solvent	Experimental	TD–HSEH1PBE/6–311G(d,p)/LanL2DZ			
	λ (nm)	λ (nm)	Osc. strength	Major contribution	
Complex **1**					
Ethanol		577	0.0584	H→L+1 (+73%)	H→L+2 (+19%)
		295	0.3590	H–1→L (+94%)	
	275	274	0.0589	H–1→L+1 (+98%)	
		242	0.0013	H–3→L+1 (+96%)	
	211	213	0.0027	H–3→L+2 (+86%)	
Gas phase		591	0.0073	H→L+2 (+46%)	H→L+1 (+28%)
		290	0.1465	H–2→L (+31%)	H–3→L (+27%)
		270	0.0098	H–1→L+1 (+84%)	
		246	0.0013	H–6→L (+88%)	
		214	0.0366	H–5→L+2 (+58%)	
Complex **2**					
Ethanol	529	598	0.0020	H→L (+93%)	
	349	469	0.0069	H→L+1 (+87%)	
	288	335	0.0021	H→L+2 (+69%)	
	263	317	0.0084	H–1→L+2 (+60%)	H–4→L+2 (+16%)
	253	294	0.1454	H→L+3 (+63%)	
	210	284	0.0078	H–15→L+1 (+39%)	H–5→L+2 (+14%)
Gas phase		622	0.0043	H→L (+66%)	H–5→L (+8%)
		477	0.0074	H→L+1 (+57%)	
		356	0.0028	H–11→L (+71%)	
		321	0.0152	H–17→L (+39%)	H–2→L+3 (+14%)
		297	0.0135	H–16→L+1 (+24%)	H–15→L+1 (+13%)
		294	0.0078	H–14→L+1 (+20%)	H–3→L+3 (+18%)
Complex **3**					
Ethanol		587	0.0003	H–2→L α (+77%)	
		492	0.0004	H–3→L α (+76%)	H–5→L α (+18%)
	285	352	0.0004	H–2→L β (+67%)	H–3→L β (+14%)
	250	329	0.0161	H–1→L+1 α (+52%)	H→L+2 β (+21%)
	227	307	0.0043	H–14→L α (+40%)	H–15→L α (+13%)
Gas phase		571	0.0062	H→L+1 β (+29%)	H–2→L+1 β (+14%)
		501	0.0003	H–2→L+1 α (+93%)	
		352	0.0007	H–3→L β (+69%)	
		340	0.0017	H–4→L β (+55%)	
Complex **4**					
Ethanol		520	0.0002	H–9→L β (+27%)	H–8→L β (+14%)
	292	294	0.0010	H→L α (+95%)	
		283	0.4419	H–1→L α (+38%)	H→L+1 β (+38%)
	249	252	0.0006	H–6→L+1 β (+80%)	
	219	248	0.0009	H–7→L α (+86%)	
Gas phase		532	0.0017	H→L β (+27%)	H–6→L β (+20%)
		295	0.0164	H–13→L β (+63%)	H–7→L α (+18%)
		280	0.0033	H–8→L+1 β (+30%)	
		275	0.2076	H–7→L+1 β (+42%)	H–8→L α (+28%)
Complex **5**					
Ethanol		314	0.0004	H→L+1 (+62%)	H–1→L+2 (+30%)
		302	0.0013	H→L (+96%)	
	275	274	0.1409	H–2→L (+68%)	H–4→L (+21%)
		252	0.0022	H→L+3 (+96%)	
	202	222	0.0055	H–7→L+3 (+61%)	H–4→L+4 (+10%)
Gas phase		408	0.0003	H→L (+100%)	
		317	0.0001	H→L+1 (+96%)	
		283	0.0004	H–1→L+4 (+93%)	
		270	0.2626	H–8→L (+81%)	
		235	0.0014	H–3→L+5 (+37%)	H–2→L+6 (+28%)
Complex **6**					
Ethanol		578	0.0003	H–16→L β (+41%)	H–22→L β (+30%)
		368	0.0001	H–23→L β (+99%)	
		331	0.0001	H–19→L α (+37%)	H–19→L+1 β (+18%)
	299	302	0.0003	H→L+3 α (+38%)	H–1→L+4 β (+38%)
	218	293	0.0002	H→L α (+27%)	H–1→L+2 β (+13%)
Gas phase		591	0.0019	H–15→L β (+35%)	H–21→L β (+35%)
		364	0.0001	H–1→L+2 β (+60%)	H–2→L+2 β (+8%)
		334	0.0001	H→L+1 β (+59%)	H–3→L+1 β (+10%)
		303	0.0001	H→L α (+36%)	H–3→L+3 β (+10%)
		297	0.0004	H–3→L+1 β (+29%)	H–1→L α (+18%)

3.5. *In vitro α-Glucosidase inhibition*

The IC_{50} values of the synthesized complexes (**1**–**6**) for α-glucosidase (from *Saccharomyces cerevisiae*, EC No: 3.2.1.20) inhibitions are given in Table 4. The results showed that the complexes **1**–**6** inhibited the α-glucosidase with IC_{50} values of 0.4699 μM and >600 μM range. Complex **6** [Hg(6-mpa)(dmdpy)$(NO_3)_2$]·H_2O has the highest α-glucosidase inhibitory activity with IC_{50} values of 0.4699 μM, which is 1928.07-fold, 35.27-fold and 27.03-fold higher than that of acarbose

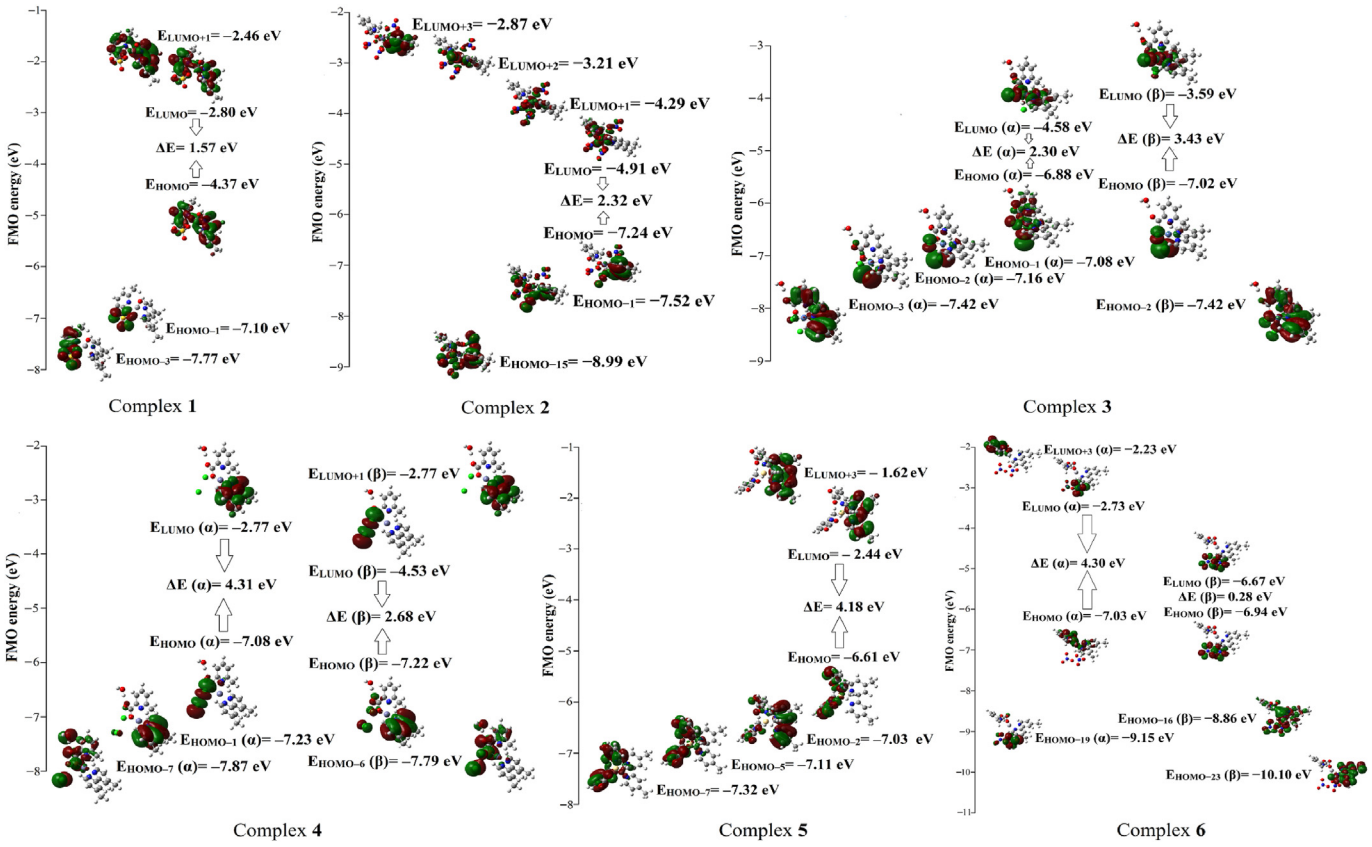

Fig. 3. The most active occupied and unoccupied molecular orbitals in electronic transition of the complexes 1–6 obtained at HSEh1PBE/6-311G(d,p)/LanL2DZ level.

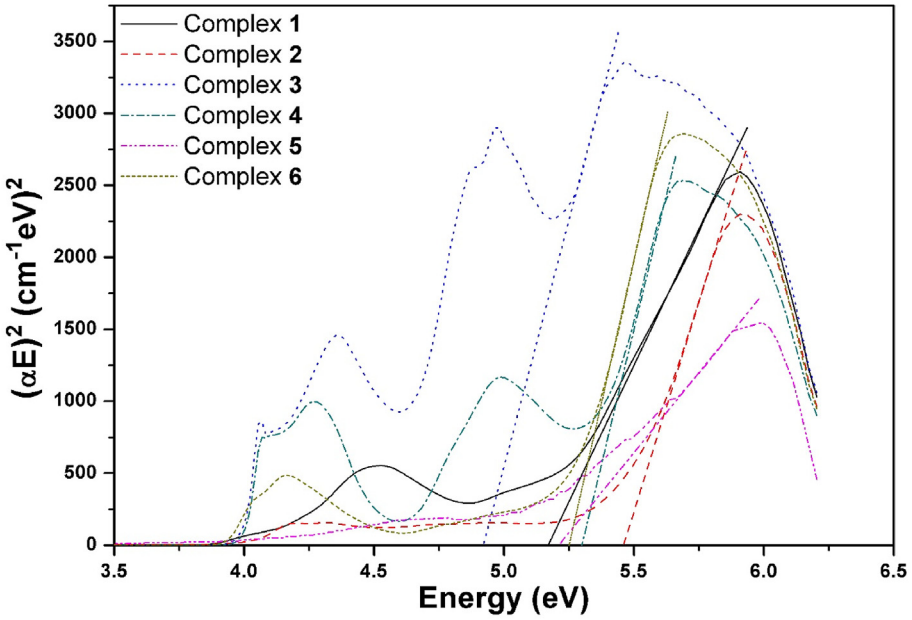

Fig. 4. The graphs of optical band gap energy for the complexes **1**–**6**.

(IC_{50} = 906 μM) [59,60], genistein (IC_{50} = 16.575 μM), and resveratrol (IC_{50} = 12.70 μM) [61,62], respectively.

The structure-activity relationship (SAR) of the synthesized complexes on α-glucosidase inhibition could be explained at the following points:

(i) The complexes **2**–**6** have the same coordination geometry as distorted octahedral geometry. Complex **6** containing Hg metal showed the strongest inhibitory activity (IC_{50} = 0.4699 μM) while the others displayed a moderate α-glucosidase inhibition. Hg complex is bulkier than the other

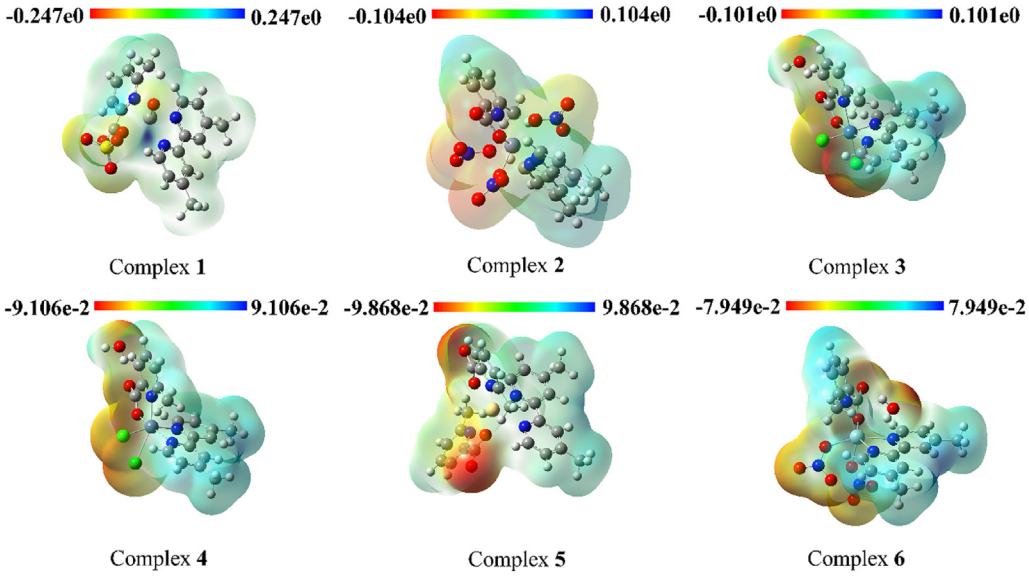

Fig. 5. Molecular electrostatic potential (MEP) surfaces for the complexes **1**–**6** obtained at HSEh1PBE/6-311G(d,p)/LanL2DZ level in gas phase.

Table 3
Electric dipole moment (μ, in Debye), the average and anisotropic static polarizabilities (⟨α⟩ and Δα, in10^{-24} esu), the first– and second– order static hyperpolarizabilities (⟨β⟩, in10^{-30} esu and ⟨γ⟩, in10^{-36} esu) for complexes **1**–**6**.

Complex	μ (Debye)		<α> (esu)		Δα		<β> (esu)		<γ> (esu)	
	Ethanol	Gas phase	Ethanol	Gas phase	Ethanol	Gas phase	Ethanol	Gas phase	Ethanol	Gas phase
Complex **1**	22.1	11.8	73.3	51.7	39.7	29.8	208.0	38.4	177.2	–
Complex **2**	16.1	11.0	73.6	51.8	25.6	19.7	11.3	5.9	118.3	31.7
Complex **3**	26.0	16.8	62.5	45.9	20.3	15.5	23.6	15.3	124.2	44.6
Complex **4**	27.1	16.1	57.5	42.6	13.5	15.1	9.2	6.8	62.7	27.8
Complex **5**	21.0	12.4	63.2	48.2	5.4	5.5	1.9	1.0	94.2	35.4
Complex **6**	23.3	13.8	85.0	71.2	56.5	35.3	657.7	435.1	36214.3	–
	6.20[a]		17[a]				9.2[a], 0.13[b]		15[a]	

[a] pNA [57,58].
[b] Urea [56].

Table 4
In vitro inhibition IC_{50} values (μM) of the complexes **1**–**6** for α–glucosidase.

Compound	IC_{50} (μM)[a]
6-methylpyridine-2-carboxylic acid (6-mpaH)	not active
4,4′-dimethyl-2,2′-bipyridyl (dmdpy)	not active
Complex **1** [VO(6-mpa)(dmdpy)]·SO_3	>600
Complex **2** [Fe(6-mpa)(dmdpy)$(NO_3)_2$]·NO_3	492.3 ± 1.05
Complex **3** Ni(6-mpa)(dmdpy)Cl_2	>600
Complex **4** [Zn(6-mpa)(dmdpy)Cl_2]·H_2O	>600
Complex **5** Cd(6-mpa)$_2$(dmdpy)	>600
Complex **6** [Hg(6-mpa)(dmdpy)$(NO_3)_2$]·H_2O	0.4699 ± 0.02
Genistein	16.575 ± 0.23
Acarbose[b]	906
Resveratrol[c]	12.70

[a] IC_{50} values represent the means ± S.E.M. of three parallel measurements ($p < 0.05$).
[b] From ref. [59,60].
[c] From ref. [61,62].

complexes due to the fact that the atomic diameter of Hg metal is larger than that of Fe, Ni, Zn and Cd metals. This difference influences on α-glucosidase inhibition.

(ii) The variation of metals (Ni, Zn and Cd) and ligand in coordination did not affect the inhibition activity (IC_{50} = >600 μM for complexes **3**–**5**) whereas the complex **2** including Fe metal showed better inhibitory activity (IC_{50} = 492.3 μM). It could be considered that the presence of nitrate ligands in coordination increased the inhibitory activity of the complex **2.**

(iii) The complex **1** consists of V=O, 6-mpa, dmbpy ligands and SO_3 molecule and it has a distorted square-bipyramidal coordination form. This difference in coordination geometry did not any affect enzyme inhibition.

It was reported that the picolinate (pa) derivatives ($Cu(pa)_2$, $Zn(pa)_2$, $VO(pa)_2$ [63] and $Zn(6mpa\text{-}ma)_2SO_4$ [64]) were synthesized as α-glucosidase inhibitors and their IC_{50} values were obtained at 1.28 μM, 15.4 μM, >1 mM, 7.5 μM, respectively. Moreover, in our previous studies, α-glucosidase inhibition values of metal complexes containing 6-mpa with cyanate, 4(5)methylimidazole, 2,2′-bipyridyl, 2,2′-dipyridylamine ligands were found to be range from 0.184 μM to >600 μM [19,24,35,36]. In this study, the complex **6** including Hg metal, as similar to previous work [35], exhibited the strongest inhibitory activity against α-glucosidase.

3.6. Docking study

Molecular docking study was fulfilled to determine the protein-ligand interactions between the synthesized complexes (**1**–**6**) and target protein (the template structure *S. cerevisiae* isomaltase(PDBID: 3A4A)). The docking results were evaluated with the electrostatic (E), hydrogen-bonding (H), and van der Waals (V) interactions for the protein-complex profiles. The estimated interactions and energy values between complex structures and amino acid residues were tabulated in Table S3. 3-D structures

showing interactions between main-/side-chain amino acids and ligand of the complexes **1**–**6** were given in Fig. 6. Fig. 6 displays interactions between complex structures and amino acid residues with regard to some hydrogen-bonding and van der Waals interactions. It is clear that the variation of metals and ligands in coordination as well as non-coordinated parts of ligands influences on the energy values of V interactions.

Complex **6** (IC_{50} = 0.4699 μM), including the Hg metal, displayed the best inhibitory activity among the substitute dmbpy ligand metal complexes. Based on docking results, the E_{total} (total energy) value of complex **6** was obtained at −124.4 kcal/mol and that of Hg(II) metal complex containing 6-mpa with 2,2′-bipyridyl ligand was found to be −93.0 kcal/mol [35]. It is observed that the ratio between these energy values is changed at least as much as the ratio of the enzyme activity results of these two complexes containing Hg metal atoms. The E_{total} values for other Fe, Ni, Zn and Cd metal complexes, which are the same coordination geometry, were calculated range from −93.6 to −116.7 kcal/mol, it could be deduced that this difference does not have a major effect on α-glucosidase inhibition. But, this difference for complex **2** affects α-glucosidase inhibition depending on coordination environment of Fe metal ion.

According to our previous docking results, the total hydrogen bonding interaction energy values of metal complexes containing 6-mpa with cyanate, 4(5)Methylimidazole, 2,2′-bipyridyl, 2,2′-dipyridylamine ligands [19,24,35,36] were obtained at the range of −27.83 and −3.5 kcal/mol depending on the same or different amino acid residues interactions. In the present study, these energies of complexes **1**–**6** were found to be range from −31.2 to −3.5 kcal/mol. Meanwhile, the minimum total energy value shows strong hydrogen bonding interaction between amino acid residues obtained at −31.2 kcal/mol for complex **6** exhibited the highest α-glucosidase inhibitory activity with IC_{50} values of 0.4699 μM. It could be concluded that these interactions for complexes **1**–**6** arise from between the carbonyl oxygen atom of 6-mpa ligand or O atom of nitrate ligand and O^{δ}, N^{δ}, N^{ξ} of same or different amino acid residues. In exemplify, the effective H-interactions were defined among the S (side chain)-ASP242 O^{δ}, S–HIS280 N^{δ}, S-TYR158 O^{η} and O atom of nitrate ligand obtained at 2.64, 3.07 and 3.08 Å bond distances, respectively. Furthermore, 6-mpa and dmbpy ligand-based docking study was fulfilled, the interactions between the amino acid residues and ligands in different energy values were observed with similar complex-protein interactions. The main reason for energy differences could be interpreted as the variation of inhibition values.

4. Conclusion

The synthesized novel metal complexes including 4,4′-dimethyl-2,2′-bipyridyl and 6-methylpyridine-2-carboxylic {[VO(6-mpa)(dmdpy)]·SO_3, (**1**), [Fe(6-mpa)(dmdpy)$(NO_3)_2$]·NO_3, (**2**), Ni(6-mpa)(dmdpy)Cl_2, (**3**), [Zn(6-mpa)(dmdpy)Cl_2]·H_2O, (**4**), Cd(6-mpa)$_2$(dmdpy), (**5**), [Hg(6-mpa)(dmdpy)$(NO_3)_2$]·H_2O, (**6**)} as potential α-glucosidase inhibitors were investigated for the first time. Their structural characterizations and spectral properties were performed by elemental analysis, LC-MS/MS, FT–IR and UV–Vis spectroscopic techniques. The α-glucosidase inhibitory activity of the synthesized complexes (**1**–**6**) were determined by IC_{50} values in the range of 0.4699 and > 600 μM. Considering these results, it could be noted that complex **6**, which shows the strongest inhibitory activity against α-glucosidase (from *Saccharomyces cerevisiae*, EC No: 3.2.1.20) is a potential α-glucosidase inhibitor candidate. In addition, the theoretical calculations with the TD/DFT-HSEh1PBE/6-311G(d,p)/LanL2DZ level were carried out to examine the detailed structural and spectral properties, as well as second- and third-order nonlinear optical parameters. The results of experimental and theoretical electronic spectra for the complexes **1**–**6** were assigned as $n\rightarrow\pi^*$ and $\pi\rightarrow\pi^*$ transitions originated from metal–ligand and ligand–ligand charge transfer. NBO results verify the coordination environment with the delocalization

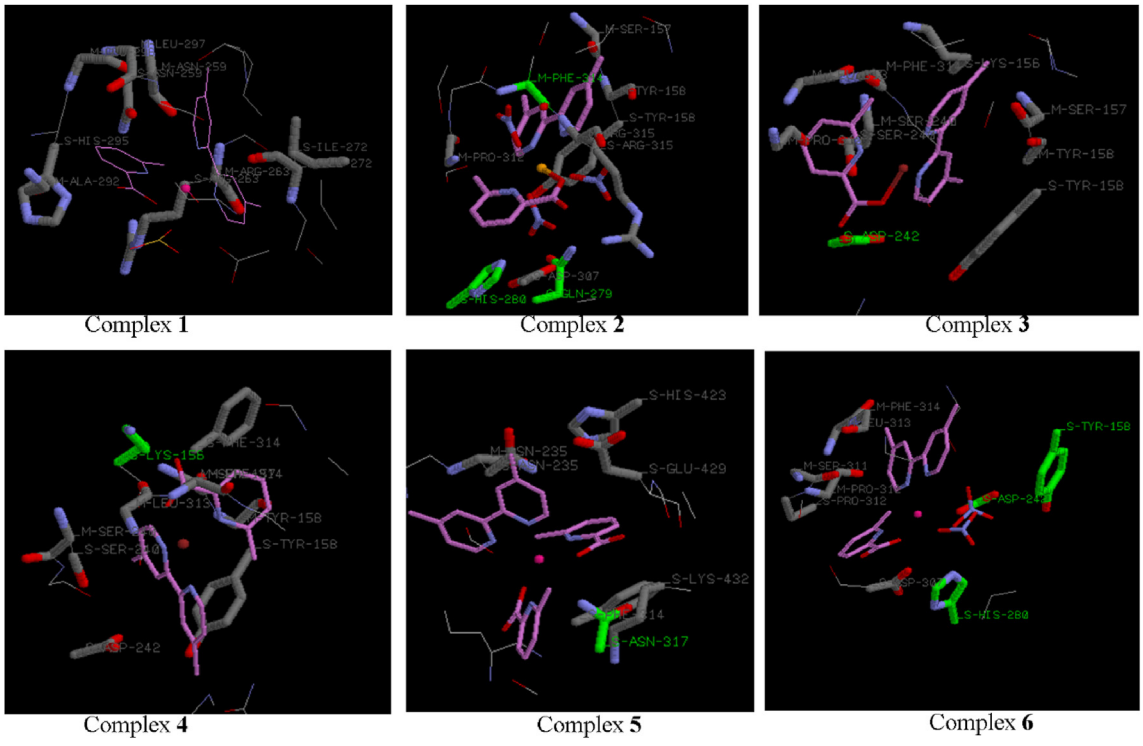

Fig. 6. 3-D structures showing interactions between main/side chain amino acids and ligand of the complexes 1–6.

effect observed between lone-pair (n) orbitals of oxygen/nitrogen atom and anti-lone-pair (n*) orbitals of metal ions. It is determined that there is a good agreement between the theoretical and corresponding experimental results. The NLO results are indicated that the complex **6** potentially a candidate for microscopic second−order and third−order NLO material. From the experimental and theoretical results, it is concluded that complex **6** is a novel and powerful drug candidate for DM II, and a remarkable scientific report for mixed-ligand metal complexes containing 6-mpa and dmbpy.

Acknowledgements

This work was supported by the Scientific and Technological Research Council of Turkey (TÜBİTAK) (Project Number: MFAG−117F235).

Appendix A. Supplementary data

Supplementary data to this article can be found online at https://doi.org/10.1016/j.molstruc.2019.127655.

References

[1] E.C. Constable, P.J. Steel, N.N′-Chelating biheteroaromatic ligands; a survey, Coord. Chem. Rev. 93 (1989) 205−223.
[2] H. Adams, N.A. Bailey, J.D. Crane, D.E. Fenton, J.M. Latour, J.M. Williams, Manganese (II) and iron (III) complexes of the tridentate ligands bis (benzimidazol−2−ylmethyl)−amine (L1) and−methylamine (L_2). Crystal structures of [MnL_1 (CH_3CO_2)$_2$],[FeL_2Cl_3], and [Fe_2L_{12} (μ−O){μ−(CH_3)$_3$ CCO_2}$_2$] [ClO_4]$_2$, J. Chem. Soc., Dalton Trans. 5 (1990) 1727−1735.
[3] W.L. Driessen, R.A.G. De Graaff, F.J. Parlevliet, J. Reedijk, R.M. De Vos, Transition metal compounds of the tridentate pyrazole substituted amine ligand bis (2− (3,5−dimethyl−1−pyrazolyl) ethyl) ethylamine (ddae). X−ray structures of [Co(ddae)(NO_3)$_2$], [Cu(ddae)(NO_3)(H_2O)](NO_3) and [Cu(ddae)(Cl)$_2$]·C_2H_5OH, Inorg. Chim. Acta 216 (1) (1994) 43−49.
[4] M. Gollapalli, M. Taha, M.T. Javid, N.B. Almandil, F. Rahim, A. Wadood, A. Mosaddik, M. Ibrahim, M.A. Alqahtani, Y.A. Bamarouf, Synthesis of benzothiazole derivatives as a potent α-glucosidase inhibitor, Bioorg. Chem. 85 (2019) 33−48.
[5] U. Ghani, Re-exploring promising a-glucosidase inhibitors for potential development into oral anti-diabetic drugs: finding needle in the haystack, Eur. J. Med. Chem. 103 (2015) 133−162.
[6] K.D. Demadis, S.D. Katarachia, Metal−phosphonate chemistry: synthesis, crystal structure of calcium−amino tris− (methylene phosphonate) and inhibition of $CaCO_3$ crystal growth, Phosphorus, Sulfur, Silicon 179 (3) (2004) 627−648.
[7] J. Monot, M. Petit, S. M Lane, I. Guisle, J. Léger, C. Tellier, D.R. Talham, B. Bujoli, Towards zirconium phosphonate−based microarrays for probing DNA− protein interactions: critical influence of the location of the probe anchoring groups, J. Am. Chem. Soc. 130 (19) (2008) 6243−6251.
[8] J. Umeda, M. Suzuki, M. Kato, M. Moriya, W. Sakamoto, T. Yogo, Proton conductive inorganic−organic hybrid membranes functionalized with phosphonic acid for polymer electrolyte fuel cell, J. Power Sources 195 (18) (2010) 5882−5888.
[9] B.Y. Saito, J. Takemoto, B. Hutchinson, K. Nakamoto, Infrared studies of coordination compounds containing low-oxidation- state metals. I. Tris(2,2′-bipyridine) and tris(1,l0-phenanthroline) complexes, Inorg. Chem. 11 (9) (1972) 2003−2011.
[10] V. Amani, N. Safari, H.R. Khavasi, Synthesis, characterization and crystal structure determination of iron(III) hetero-ligand complexes containing 2,2′-bipyridine, 5,5′-dimethyl-2,2′-bipyridine and chloride, [Fe(bipy)Cl_4][bipy·H] and [Fe(dmbipy)$_2$$Cl_2$][$FeCl_4$], Polyhedron 26 (2007) 4257−4262.
[11] S.M. Mobin, A.K. Saini, V. Mishra, A. Chaudhary, A series of new heteroleptic Hg(II) complexes: synthesis, crystal structures and photophysical properties, Polyhedron 110 (2016) 131−141.
[12] Ö. Tamer, S. Arabacı Tamer, Ö. İdil, D. Avcı, H. Vural, Y. Atalay, Antimicrobial activities, DNA interactions, spectroscopic (FT-IR and UV-Vis) characterizations, and DFT calculations for pyridine-2-carboxylic acid and its derivates, J. Mol. Struct. 1152 (2018) 399−408.
[13] Li-N. Zhu, Ya-W. Jin, Xiao-Z. Li, J. Wang, De-M. Kong, Huai-F. Mi, Dai-Z. Liao, Han-X. Shen, Synthesis, structure and DNA cleavage activity of two 4,4′-dimethyl-2,2′-bipyridyl manganese(II) complexes, Inorg. Chim. Acta 361 (2008) 29−35.
[14] Li-J. Yang, Qing-L. Liu, Ming-X. Wang, Lian-S. Gu, Yang-H. Luo, Bai-W. Sun, Complexation of different transition metals with 4,4′-dimethyl-2,2′-bipyridine: crystal structure, UV spectra and Hirshfeld surfaces, Spectrochim. Acta A 166 (2016) 1−7.
[15] M. Barquín, N. Cocera, M.J. González Garmendia, L. Larrínaga, E. Pinilla, J.M. Seco, M.R. Torres, Acetato and formato copper(II) complexes with 4,4′-dimethyl-2,2′-bipyridine and 5,5′-dimethyl-2,2′-bipyridine: synthesis, crystal structure, magnetic properties and EPR results. A new 1D polymeric water chain, Inorg. Chim. Acta 363 (2010) 127−133.
[16] C.M.M. Santos, M. Freitas, E. Fernandes, A comprehensive review on xanthone derivatives as α-glucosidase inhibitors, Eur. J. Med. Chem. 157 (2018) 1460−1479.
[17] H. Sun, Y.Z. Zhang, W.N. Ding, X. Zhao, X.T. Song, D. Wang, Y.S. Li, K.L. Han, Y. Yang, Y. Ma, R.L. Wang, D. Wang, P. Yu, Inhibitory activity evaluation and mechanistic studies of tetracyclic oxindole derivatives as alpha-glucosidase inhibitors, Eur. J. Med. Chem. 123 (2016) 365−378.
[18] A. Barakat, M.S. Islam, A.M. Al-Majid, H.A. Ghabbour, S. Yousuf, M. Ashraf, N.N. Shaikh, M.I. Choudhary, R. Khalil, Z. Ul-Haq, Synthesis of pyrimidine-2,4,6-trione derivatives: anti-oxidant, anti-cancer, alpha-glucosidase, beta-glucuronidase inhibition and their molecular docking studies, Bioorg. Chem. 68 (2016) 72−79.
[19] D. Avcı, S. Altürk, F. Sönmez, Ö. Tamer, A. Başoğlu, Y. Atalay, B.Z. Kurt, N. Dege, Three novel Cu(II), Cd(II) and Cr(III) complexes of 6-Methylpyridine-2-carboxylic acid with thiocyanate: synthesis, crystal structures, DFT calculations, molecular docking and α-Glucosidase inhibition studies, Tetrahedron 74 (2018) 7198−7208.
[20] X. Bian, X. Fan, C. Ke, Y. Luan, G. Zhao, A. Zeng, Synthesis and α-glucosidase inhibitory activity evaluation of N-substituted aminomethyl-b-D-glucopyranosides, Bioorg. Med. Chem. 21 (2013) 5442−5450.
[21] S. Adisakwattana, P. Charoenlertkul, S. Yıbchok−Anun, α−Glucosidase inhibitory activity of cyanidin−3−galactoside and synergistic effect with acarbose, J. Enzym. Inhib. Med. Chem. 24 (1) (2009) 65−69.
[22] M. Gollapalli, M. Taha, H. Ullah, M. Nawaz, L.M.R. AlMuqarrabun, F. Rahim, F. Qureshi, A. Mosaddik, N. Ahmat, K.M. Khan, Synthesis of Bis-indolylmethane sulfonohydrazides derivatives as potent α-Glucosidase inhibitors, ides derivatives as potent α-Glucosidase inhibitors, Bioorg. Chem. 80 (2018) 112−120.
[23] H. Tang, F. Ma, D. Zhao, Z. Xue, Exploring the effect of salvianolic acid C on α-glucosidase: inhibition kinetics, interaction mechanism and molecular modelling methods, Process Biochem. 78 (2019) 178−188.
[24] D. Avcı, S. Altürk, F. Sönmez, Ö. Tamer, A. Başoğlu, Y. Atalay, B.Z. Kurt, N. Dege, A novel series of M(II) complexes of 6-methylpyridine-2-carboxylic acid with 4(5) methylimidazole: synthesis, crystal structures, α-glucosidase activity, density functional theory calculations and molecular docking, Appl. Organomet. Chem. 33 (2019) e4935.
[25] D. Avcı, S. Altürk, F. Sönmez, Ö. Tamer, A. Başoğlu, Y. Atalay, B.Z. Kurt, D. Öztürk, N. Dege, A new dinuclear copper (II) complex of 2,5−Furandicarboxyclic acid with 4(5)−Methylimidazole as a high potential α−glucosidase inhibitor: synthesis, Crystal structure, Cytotoxicity study, and TD/DFT calculations, Appl. Organomet. Chem. 33 (2019), e4725.
[26] M.J. Frisch, G.W. Trucks, H.B. Schlegel, G.E. Scuseria, M.A. Robb, J.R. Cheeseman, G. Scalmani, V. Barone, B. Mennucci, G.A. Petersson, H. Nakatsuji, M. Caricato, X. Li, H.P. Hratchian, A.F. Izmaylov, J. Bloino, G. Zheng, J.L. Sonnenberg, M. Hada, M. Ehara, K. Toyota, R. Fukuda, J. Hasegawa, M. Ishida, T. Nakajima, Y. Honda, O. Kitao, H. Nakai, T. Vreven, J.A. Montgomery Jr., J.E. Peralta, F. Ogliaro, M. Bearpark, J.J. Heyd, E. Brothers, K.N. Kudin, V.N. Staroverov, R. Kobayashi, J. Normand, K. Raghavachari, A. Rendell, J.C. Burant, S.S. Iyengar, J. Tomasi, M. Cossi, N. Rega, J.M. Millam, M. Klene, J.E. Knox, J.B. Cross, V. Bakken, C. Adamo, J. Jaramillo, R. Gomperts, R.E. Stratmann, O. Yazyev, A.J. Austin, R. Cammi, C. Pomelli, J.W. Ochterski, R.L. Martin, K. Morokuma, V.G. Zakrzewski, G.A. Voth, P. Salvador, J.J. Dannenberg, S. Dapprich, A.D. Daniels, O. Farkas, J.B. Foresman, J.V. Ortiz, J. Cioslowski, D.J. Fox, Gaussian 09, Revision D.01, Gaussian, Inc., Wallingford, CT, 2013.
[27] R. Dennington, T. Keith, J. Millam, GaussView, Version 5, Semichem Inc., Shawnee Mission KS, 2009.
[28] J. Heyd, G.E. Scuseria, Efficient hybrid density functional calculations in solids: assessment of the Heyd-Scuseria-Ernzerhof screened Coulomb hybrid functional, J. Chem. Phys. 121 (2004) 1187−1192.
[29] A.V. Krukau, O.A. Vydrov, A.F. Izmaylov, G.E. Scuseria, Influence of the exchange screening parameter on the performance of screened hybrid functionals, J. Chem. Phys. 125 (2006) 224106.
[30] M.J. Frisch, J.A. Pople, J.S. Binkley, Self-consistent molecular orbital methods 25. Supplementary functions for Gaussian basis set, J. Chem. Phys. 80 (1984) 3265−3269.
[31] P.J. Hay, W.R. Wadt, Ab initio effective core potentials for molecular calculations. Potentials for the transition metal atoms Sc to Hg, J. Chem. Phys. 82 (1985) 270−283.
[32] E. Runge, E.K.U. Gross, Density-functional theory for time-dependent systems, Phys. Rev. Lett. 52 (1984) 997−1000.
[33] S. Miertus, E. Scrocco, J. Tomasi, Electrostatic interaction of a solute with a continuum. A direct utilizaion of Ab initiomolecular potentials for the prevision of solvent effects, J. Chem. Phys. 55 (1981) 117−129.
[34] J.-M. Yang, C.-C. Chen, GEMDOCK: a generic evolutionary method for molecular docking, Proteins 55 (2004) 288−304.
[35] D. Avcı, S. Altürk, F. Sönmez, Ö. Tamer, A. Başoğlu, Y. Atalay, B. Zengin Kurt, N. Dege, A novel series of mixed-ligand M(II) complexes containing 2,2′-bipyridyl as potent α-glucosidase inhibitor: synthesis, crystal structure, DFT

calculations, and molecular docking, JBIC J. Biolog. Inorg. Chem. (2019), https://doi.org/10.1007/s00775-019-01688-9.
[36] D. Avcı, S. Altürk, F. Sönmez, Ö. Tamer, A. Başoğlu, Y. Atalay, B. Zengin Kurt, N. Dege, Novel Cu(II), Co(II) and Zn(II) metal complexes with mixed-ligand: synthesis, crystal structure, α-glucosidase inhibition, DFT calculations, and molecular docking, J. Mol. Struct. 1197 (2019) 645–655.
[37] S. Altürk, D. Avcı, A. Başoğlu, Ö. Tamer, Y. Atalay, N. Dege, Copper(II) complex with 6-methylpyridine-2-carboxyclic acid: experimental and computational study on the XRD, FT-IR and UV–Vis spectra, refractive index, band gap and NLO parameters, Spectrochim. Acta A Mol. Biomol. Spectrosc. 190 (2018) 220–230.
[38] A.E. Reed, F. Weinhold, Natural bond orbital analysis of near-Hartree–Fock water dimer, J. Chem. Phys. 78 (1983) 4066–4073.
[39] J.P. Foster, F. Weinhold, Natural hybrid orbitals, J. Am. Chem. Soc. 102 (1980) 7211–7218.
[40] A.P. Scott, L. Radom, Harmonic vibrational frequencies: an evaluation of Hartree-Fock, Møller-Plesset, quadratic configuration interaction, density functional theory, and Semiempirical scale factors, J. Phys. Chem. 100 (1996) 16502–16513.
[41] B.-M. Kukovec, Z. Popović, B. Kozlevčar, Z. Jagličić, 3D supramolecular architectures of copper(II) complexes with 6-methylpicolinic and 6-bromopicolinic acid: synthesis, spectroscopic, thermal and magnetic properties, Polyhedron 27 (2008) 3631–3638.
[42] B.-M. Kukovec, P.D. Vaz, Z. Popović, M.J. Calhorda, K. Furić, G. Pavlović, M.R. Linarić, Pseudopolymorphismin nickel(II) complexes with 6-methylpicolinic acid. Synthesis, structural, spectroscopic, thermal and DFT study, Cryst. Growth Des. 8 (2008) 3465–3473.
[43] J. Pons, R. March, J. Rius, J. Ros, Zinc complexes of 6-methyl-2-pyridinecarboxylic acid. Crystal structure of $[Zn(MeC_5H_3NCOO)_2(H_2O)]\cdot H_2O$, Inorg. Chim. Acta 357 (2004) 3789–3792.
[44] R. Alizadeh, V. Amani, Syntheses, crystal structures, and photoluminescence of three cadmium(II) coordination complexes based on bipyridine ligands with different positioned methyl substituents, Inorg. Chim. Acta 443 (2016) 151–159.
[45] M. Belicchi-Ferrari, F. Bisceglie, C. Cavalieri, G. Pelosi, P. Tarasconi, Bis(-triphenylphosphine)4-fluorobenzaldehyde thiosemicarbazone copper(I): forcing chelation through oxoanions, Polyhedron 26 (2007) 3774–3782.
[46] S.I. Gorelsky, SWizard Program Revision 4.5, University of Ottawa, Ottawa, Canada, 2010. http://www.sg.chem.net/.
[47] İ. Şişman, A. Başoğlu, Effect of Se content on the structural, morphological and optical properties of $Bi_2Te_{3-y}Se_y$ thin films electrodeposited by under potential deposition technique, Mater. Sci. Semicond. Process. 54 (2016) 57–64.
[48] W. Yang, R.G. Parr, Hardness, softness, and the fukui function in the electronic theory of metals and catalysis, Proc. Nati. Acad. Sci. USA 82 (1985) 6723–6726.
[49] J. Sponer, P. Hobza, DNA base amino groups and their role in molecular interactions: ab initio and preliminary density functional theory calculations, Int. J. Quantum Chem. 57 (1996) 959–970.
[50] S.R. Gadre, I.H. Shrivastava, Shapes and sizes of molecular anions via topographical analysis of electrostatic potential, J. Chem. Phys. 94 (1991) 4384–4390.
[51] D.S. Chemla, J. Zysss, Nonlinear Optical Properties of Organic Molecules and Crystals, Academic Press, Orlando, FL, 1987.
[52] K. Kamada, M. Ueda, H. Nagao, K. Tawa, T. Sugino, Y. Shmizu, K. Ohta, Molecular design for organic nonlinear optics: polarizability and hyperpolarizabilities of furan homologues investigated by ab initio molecular orbital method, J. Phys. Chem. A 104 (2000) 4723–4734.
[53] B.M. Pierce, A theoretical analysis of third-order nonlinear optical properties of linear polyenes and benzene, J. Chem. Phys. 91 (1989) 791–811.
[54] S. Altürk, D. Avcı, Ö. Tamer, Y. Atalay, O. Şahin, A cobalt(II) complex with 6-methylpicolinate: synthesis, characterization, second- and third-order nonlinear optical properties, and DFT calculations, J. Phys. Chem. Solids 98 (2016) 71–80.
[55] F. Castet, V. Rodriguez, J.-L. Pozzo, L. Ducasse, A. Plaquet, B. Champagne, Design and characterization of molecular nonlinear optical switches, Acc. Chem. Res. 46 (2013) 2656–2665.
[56] C. Adant, M. Dupuis, J.L. Bredas, Ab initio study of the nonlinear optical properties of urea: electron correlation and dispersion effects, Int. J. Quantum Chem. 56 (2004) 497–507.
[57] L.-T. Cheng, W. Tam, S.H. Stevenson, G.R. Meredith, G. Rikken, S.R. Marder, Experimental investigations of organic molecular nonlinear optical polarizabilities. 1. Methods and results on benzene and stilbene derivatives, J. Phys. Chem. 95 (1991) 10631–10643.
[58] P. Kaatz, E.A. Donley, D.P. Shelton, A comparison of molecular hyperpolarizabilities from gas and liquid phase measurements, J. Chem. Phys. 108 (1998) 849–856.
[59] M. Taha, N. Hadiani Ismail, S. Lalani, M. Qaiser Fatmi, Atia-tul-Wahab, S. Siddiqui, K.M. Khan, S. Imran, M. Iqbal Choudhary, Synthesis of novel inhibitors of α-glucosidase based on the benzothiazole skeleton containing benzohydrazide moiety and their molecular docking studies, Eur. J. Med. Chem. 92 (2015) 387–400.
[60] M. Taha, N. Hadiani Ismail, M. Syukri Baharudin, S. Lalani, S. Mehboob, K.M. Khan, S. Yousuf, S. Siddiqui, F. Rahim, M.I. Choudhary, Synthesis crystal structure of 2-methoxybenzoylhydrazones and evaluation of their α-glucosidase and urease inhibition potential, Med. Chem. Res. 24 (2015) 1310–1324.
[61] J.-W. Zheng, L. Ma, Silver(I) complexes of 2,4-dihydroxybenzaldehyde–amino acid Schiff bases-Novel noncompetitive α-glucosidase inhibitors, Bioorg. Med. Chem. Lett 25 (2015) 2156–2216.
[62] J.-W. Zheng, L. Ma, Metal complexes of anthranilic acid derivatives: a new class of non-competitive α-glucosidase inhibitors, Chin. Chem. Lett. 27 (2016) 627–630.
[63] Y. Yoshikawa, R. Hirata, H. Yasui, H. Sakurai, Alpha–glucosidase inhibitory effect of anti–diabetic metal ions and their complexes, Biochimie 91 (2009) 1339–1341.
[64] E. Ueda, Y. Yoshikawa, H. Sakurai, Y. Kojima, N.M. Kajiwara, In vitro α-glucosidase inhibitory effect of Zn(II) complex with 6-methyl-2-picolinmethylamide, Chem. Pharm. Bull. 53 (4) (2005) 451–452.